



ChemComm

**Active site separation of photocatalytic steam reforming of methane using Gas-Phase Photoelectrochemical system**

Journal:	<i>ChemComm</i>
Manuscript ID	CC-COM-06-2021-002914.R1
Article Type:	Communication

SCHOLARONE™  
Manuscripts

## COMMUNICATION

## Active site separation of photocatalytic steam reforming of methane using Gas-Phase Photoelectrochemical system

Tomoki Kujirai,<sup>a</sup> Akira Yamaguchi\*,<sup>a</sup> Takeshi Fujita,<sup>b</sup> Hideki Abe<sup>c</sup> and Masahiro Miyauchi\*<sup>a</sup>

Received 00th January 20xx,  
Accepted 00th January 20xx

DOI: 10.1039/x0xx00000x

**Steam reforming of methane (SRM) requires high temperatures to be promoted, and the production of carbon dioxide from the side reaction has also become a problem. In this study, we separated the reaction sites for SRM to suppress CO<sub>2</sub> generation using a gas-phase photoelectrochemical (GPEC) system with a cell coated with Pt/YSZ powder catalyst on an oxygen ions-conductive YSZ pellet, where the reaction was assisted by light irradiation. As a result, SRM proceeded stoichiometrically and the production of CO<sub>2</sub> was suppressed. We expect the findings obtained by the GPEC system will be useful in providing design guidelines for photocatalysts.**

Methane (CH<sub>4</sub>) is an extremely stable hydrocarbon molecule that exists abundantly on Earth as a natural resource in the form of natural gas, shale gas, and methane hydrates. According to the U.S. Energy Information Administration, the amount of shale gas which is extracted from shale formations is increasing every year due to recent developments in mining technology.<sup>1</sup> Also, CH<sub>4</sub> emitted into the atmosphere is the second most influential greenhouse gas after carbon dioxide (CO<sub>2</sub>).<sup>2</sup> Because CH<sub>4</sub> exists in abundance on the earth, it is expected to be an important energy source and also a cause of global warming. Conversion of CH<sub>4</sub> into useful chemical raw materials through steam reforming of methane (SRM; CH<sub>4</sub>+H<sub>2</sub>O →CO+3H<sub>2</sub>, ΔH<sub>298K</sub>=+205 kJ/mol), dry reforming of methane (DRM; CH<sub>4</sub>+CO<sub>2</sub> →2CO+2H<sub>2</sub>, ΔH<sub>298K</sub>=+247 kJ/mol), and partial oxidation of methane (POM; CH<sub>4</sub>+1/2 O<sub>2</sub> →CO+2H<sub>2</sub>, ΔH<sub>298K</sub>=-38 kJ/mol),<sup>3</sup> are promising.<sup>4</sup> SRM and DRM are useful reactions to produce hydrogen (H<sub>2</sub>) and carbon monoxide (CO), which are raw materials for many chemical products, from greenhouse gases. However, they require high temperatures to be promoted because they are highly endothermic reactions.<sup>3,5,6</sup> To promote these endothermic reactions at lower operating temperatures,

harnessing light energy and renewable energy using photocatalysts is one of the strategies.<sup>7</sup>

Various studies have been conducted on the use of light energy for SRM<sup>8–12</sup> and DRM<sup>9,13–15</sup>. Through investigation of the photocatalytic DRM using Rh/SrTiO<sub>3</sub> powder catalysts, Shoji et al. found that the oxygen ions (O<sup>2-</sup>) in SrTiO<sub>3</sub> acted as mediators of the oxidation (CH<sub>4</sub>+ O<sup>2-</sup> →CO+2H<sub>2</sub>+2e<sup>-</sup>) and reduction reactions (CO<sub>2</sub>+2e<sup>-</sup>→CO+O<sup>2-</sup>).<sup>16</sup> However, it is difficult to elucidate the reaction mechanism of these reactions when they are promoted by powder catalysts. This is because the oxidation and reduction sites are mixed in the catalysts. To address this issue, our group constructed a gas-phase photoelectrochemical (GPEC) system<sup>17</sup> using a solid electrolyte with oxygen ion conductivity to separate the anodic and cathodic sites. Our group then analyzed the reaction mechanism of photocatalytic DRM to propose a strategic design of the photocatalyst for the reaction.<sup>18</sup> Using this system, we can evaluate the oxidation and reduction sites separately, which had not been possible for conventional powder catalysts.

In comparison with DRM, the SRM reaction is advantageous for H<sub>2</sub> production because of the large amount of H<sub>2</sub> obtained from each molecule of CH<sub>4</sub>.<sup>19,20</sup> Yoshida et al. first reported the photocatalytic SRM using Pt/TiO<sub>2</sub>.<sup>8</sup> Ye et al. reported that hot carrier generation in noble metal nanoparticles promoted the photocatalytic SRM using Rh/TiO<sub>2</sub>.<sup>11</sup> However, the generation of CO<sub>2</sub> from the side reaction and the water gas shift (CO+H<sub>2</sub>O→CO<sub>2</sub>+H<sub>2</sub>, ΔH<sub>298K</sub>=-41 kJ/mol) is attributed to the fact that the oxidation and reduction sites are in the same place, which has become a problem. The generated CO<sub>2</sub> is a greenhouse gas that causes global warming, and its disposal is a major problem.<sup>21</sup>

In this work, we applied the GPEC system to SRM because its site-separation properties are advantageous for suppressing side reactions, CO<sub>2</sub> generation. First, we evaluated the SRM activity of a powder photocatalyst synthesized by loading Pt onto zirconium(IV) oxide stabilized yttrium oxide (YSZ) powder. Then, we evaluated the SRM properties using the GPEC system with a cell, which was fabricated by screen-printing the Pt/YSZ powder catalyst on a YSZ pellet. In this study, we aimed to

<sup>a</sup> Department of Materials Science and Engineering, Tokyo Institute of Technology, 2-12-1 Ookayama, Meguro-ku, Tokyo 152-8552, Japan.

<sup>b</sup> Department of Environmental Science and Engineering, Kochi University of Technology, 185 Miyanokuchi, Tosayamada, Kami, Kochi 782-8502, Japan

<sup>c</sup> National Institute for Materials Science, 1-1 Namiki, Tsukuba, Ibaraki 305-0044, Japan.

† Electronic Supplementary Information (ESI) available. See DOI: 10.1039/x0xx000

separate the oxidation and reduction sites in the catalyst used for SRM using the GPEC system, as shown in Figure S2, thereby suppressing the generation of CO<sub>2</sub> by side reactions. Furthermore, we analyzed the effects of light irradiation and photogenerated carriers in SRM. Electron spin resonance (ESR) measurements were performed to analyze the photogenerated carriers in the Pt/YSZ powder catalyst during light irradiation. Detailed experimental procedures are provided in the Supplementary information.

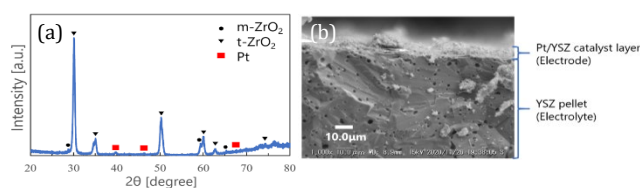
First, we discuss the characterization of the powder. Figure S8(a) shows the XRD pattern of the Pt/YSZ powder catalyst. This XRD pattern indicated that the Pt/YSZ powder catalyst consisted of two kinds of ZrO<sub>2</sub> crystal phases: monoclinic ZrO<sub>2</sub> (PDF#00-050-1089) and tetragonal- ZrO<sub>2</sub> (PDF#00-037-1484). In Figure S8(a), no metal Pt peak was observed because it was buried in the YSZ peak and background due to the small amount of Pt metal. Figure S8(b) illustrates the XRD pattern of the YSZ pellet before screen printing (bare YSZ). All peaks in this XRD pattern can be assigned to tetragonal ZrO<sub>2</sub> (PDF#00-042-1164).

Figure S9(a) shows a transmission electron microscope (TEM) image of the Pt/YSZ powder catalyst. This TEM image shows that the Pt particles were well dispersed in the YSZ powder in the Pt/YSZ powder catalyst. The loaded Pt particles were nanoparticles with sizes ranging from several nanometers to 10 nm. The EDS (Figure S9(b), (c)) results also showed the presence of Pt on the Pt/YSZ powder catalyst.

Figure S10(a) shows the UV-Vis absorption spectra of the YSZ powder and Pt/YSZ powder catalyst. The absorption spectrum of the YSZ powder shows absorption in the UV light region, which is caused by the band gap excitation of the semiconductors. Figure S10(b) shows the Tauc plot obtained from the absorption spectra of the YSZ powder shown in Figure S10(a). The band gap of the YSZ powder, as estimated by extrapolating the linear part of this Tauc plot, was  $E_g = 5.17$  eV, which is close to the previously reported band gap of YSZ (4.96 eV, 5.2 eV).<sup>22,23</sup>

Figure 1(a) shows the XRD pattern of the cell used in the GPEC system. This XRD pattern indicated that the cell consisted of two kinds of ZrO<sub>2</sub> crystal phases: monoclinic- ZrO<sub>2</sub> (PDF#00-050-1089) and tetragonal- ZrO<sub>2</sub> (PDF#00-042-1164). This suggests that the cell consisted of monoclinic- ZrO<sub>2</sub> derived from the YSZ powder and tetragonal- ZrO<sub>2</sub> derived from the YSZ pellet. The presence of Pt (PDF#00-004-0802) in the cell, as shown in Figure 1(a), suggests that the Pt precursor was reduced to the metallic phase by H<sub>2</sub> flow. The results indicate that the catalyst layer of the desired Pt/YSZ powder catalyst was formed on the YSZ pellet in the fabricated cell.

Figure 1(b) shows an SEM image of the cross section of the cell. This SEM image shows that the cell consisted of a porous



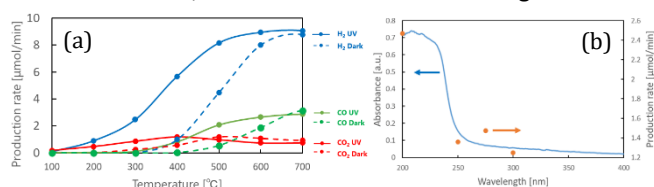
**Fig. 1** (a) The XRD pattern of the cell. (b) The SEM image of the cross section of the cell.

layer of about 10  $\mu\text{m}$  thickness made of the Pt/YSZ powder catalyst and the layer of the YSZ pellet. This catalyst layer was formed by screen-printing and was sufficiently thin and porous to fulfill the requirements of the cells used in the GPEC system.

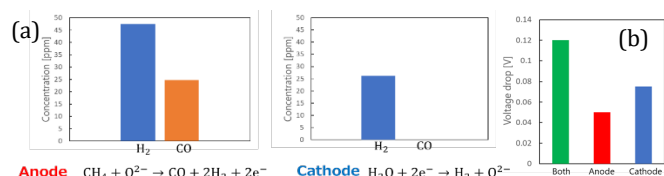
The spectrum of the Hg-Xe lamp used in this study is shown in Figure S11. Figure 2(a) illustrates the temperature dependence of the production rates of H<sub>2</sub>, CO, and CO<sub>2</sub> during photocatalytic SRM using the Pt/YSZ powder catalyst under dark conditions and UV light irradiation. This figure shows that the photocatalytic SRM activity of the Pt/YSZ powder catalyst showed a similar trend as those calculated using the thermodynamic limits of SRM, as shown in Figure S12.<sup>24</sup> The production rate of H<sub>2</sub> was higher under UV light irradiation than under dark conditions, indicating that UV light irradiation accelerated the SRM. In other words, the photocatalyst lowered the reaction temperature of the SRM and converted the incoming light energy into chemical energy. However, in the photocatalytic SRM using Pt/YSZ powder catalyst, CO<sub>2</sub> is generated due to the side reaction, water gas shift ( $\text{CO} + \text{H}_2\text{O} \rightarrow \text{CO}_2 + \text{H}_2$ ), even in the high reaction temperature region with a high production rate of H<sub>2</sub> (see Figure 2(a)). This is a major problem in powder systems, as mentioned in the introduction.

Figure 2(b) shows the action spectrum of the Pt/YSZ powder catalyst under UV light irradiation and the UV-vis absorption spectra of the YSZ powder. As seen from Figure 2(b), the trend of the action spectrum is consistent with that of the UV-vis absorption spectrum of the YSZ powder. This means that the photogenerated carriers in the YSZ powder caused by light irradiation with wavelengths shorter than approximately 240 nm, which correspond to the estimated band gap of 5.17 eV of the YSZ powder, contributed to the promotion of the SRM.

Here, we applied the GPEC system to the SRM to separate the oxidation and reduction sites. Figure 3(a) shows the concentrations of the products on the anodic and cathodic sides generated by SRM under UV light irradiation and galvanostatic conditions of 900  $\mu\text{A}$ . This figure shows that the concentration of H<sub>2</sub> generated on the anode side was almost twice that of CO on the anode side, and the concentration of H<sub>2</sub> generated on



**Fig. 2** (a) The temperature dependence of the production rates of H<sub>2</sub>, CO, and CO<sub>2</sub> during photocatalytic SRM using the Pt/YSZ powder catalyst under dark conditions and UV light irradiation. (b) The action spectrum of the Pt/YSZ powder catalyst under UV light irradiation (orange plots) and the UV-vis absorption spectra for the YSZ powder (blue line).



**Fig. 3** SRM activity conducted by GPEC system under UV light irradiation at 700 °C. (a) The concentrations of the products and (b) The voltage drop caused by the UV light irradiation.

the cathode side was almost the same as that of CO on the anode side. This result is stoichiometrically consistent with the predicted reaction of the SRM with the reaction sites separated at the anode ( $\text{CH}_4 + \text{O}^{2-} \rightarrow \text{CO} + 2\text{H}_2 + 2\text{e}^-$ ) and the cathode ( $\text{H}_2\text{O} + 2\text{e}^- \rightarrow \text{H}_2 + \text{O}^{2-}$ ). This indicates that the oxygen ions move from the cathode side to the anode side through the YSZ pellet of the cell and act as mediators for the SRM. Remarkably,  $\text{CO}_2$  generation was not evidenced on either the anode or the cathode side. This means that the separation of the reaction sites was achieved, and it succeeded in suppressing the generation of  $\text{CO}_2$  that occurred when the Pt/YSZ powder catalyst was used even at  $700^\circ\text{C}$  when the production rate of  $\text{H}_2$  was high. This is because no side reaction (water gas shift) occurred since the CO produced on the anode side did not mix with the water vapor supplied to the cathode side.

To examine the temperature rise of the cell due to UV light irradiation, we measured the surface temperature of the cell under identical conditions to those of the GPEC system. The temperature rise due to UV irradiation was only  $2^\circ\text{C}$ . This indicates that UV light irradiation had a very limited contribution to the temperature rise of the cell in the GPEC system. The GPEC system also enabled discussion on the effect of UV irradiation on the anode and cathode sides separately. Prior to the discussion, we had also investigated the effect of the transmitted light on the opposite side of the cell by looking at the spectra of the transmitted light of the cell (Figures S13(a) and (b)). These figures hint that the intensity of the light transmitted through the cell is very small compared to that irradiated from the Hg-Xe lamp. This indicates that in light irradiation experiments using the GPEC system, UV light irradiation of one side (either of the anode or cathode side) does not produce photogenerated carriers in the photocatalyst on the opposite side of the cell. Thus, the effects of UV light irradiation of the anode or cathode side can be separately discussed.

Figure 3(b) shows the voltage change caused by UV light irradiation in the SRM using the GPEC system. This measurement was performed under the same galvanostatic conditions as shown in Figure 3(a). Figure 3(b) illustrates that the voltage dropped both when solely the anode was irradiated with UV light and when solely the cathode was irradiated. The sum of the voltage drop due to UV light irradiation of solely the anode and that due to UV irradiation of solely cathode was almost equal in value to that in the case where both the anode and cathode sides were irradiated. The voltage drop under galvanostatic conditions indicates the voltage decrease that must be applied to pass the same current. In other words, the SRM was promoted by light energy from the UV light irradiation. This result enabled the description of the transfer model of photogenerated carriers shown in Figure S14, which was inferred from the ESR measurements performed on the Pt/YSZ powder catalyst (vide infra). The transfer model of photogenerated carriers can also occur under UV irradiation in separated reaction sites using the GPEC system.

To analyze the photogenerated carriers in the Pt/YSZ powder catalyst during light irradiation, ESR measurements

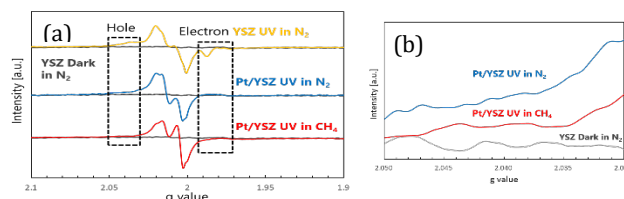
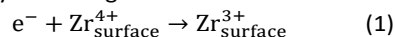


**Fig. 4** (a) The ESR spectra for the powder catalyst. (b) The decrease in the signal of holes.

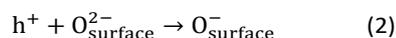
were performed using an operando electron spin resonance system. Figure 4(a) shows the ESR spectra of the powder catalyst. No signal assignable to unpaired electrons was observed in the ESR spectrum of the YSZ powder without Pt under a nitrogen ( $\text{N}_2$ ) atmosphere and dark conditions (black line). This is reasonable because a previous study reported that YSZ contains  $\text{Zr}^{4+}$  and F-type centers, proving that two electrons are trapped in an oxygen vacancy.<sup>25</sup>

Under UV light irradiation, a signal was observed around  $g = 2.00 \sim 2.02$ . This can be attributed to the  $\text{F}^-$  type centers formed by trapping of an electron by an oxygen vacancy on the surface by UV light irradiation, as suggested by the previous studies.<sup>22,26–28</sup>

In the ESR spectrum of the YSZ powder without Pt loaded under the  $\text{N}_2$  atmosphere and UV light irradiation (yellow line), a strong signal around  $g = 1.99$  and a weak signal around  $g = 1.97$  were observed. These signals can be assigned to  $\text{Zr}^{3+}$  formed by trapping of an electron in  $\text{Zr}^{4+}$  (see equation (1)), as reported in previous studies.<sup>25,27,29,30</sup> Thus, photogenerated electrons generated by the UV light irradiation caused these signals.



In the ESR spectrum of the Pt/YSZ powder catalyst under the  $\text{N}_2$  atmosphere and UV light irradiation (blue line), the signals around  $g = 1.99$ , and  $g = 1.97$  disappeared. It is considered that the signals assignable to  $\text{Zr}^{3+}$  were not observed because the photogenerated electrons had been transferred to the Pt particles in the YSZ powder with Pt loading. Under  $\text{N}_2$  conditions, a signal in the range of  $g = 2.03 \sim 2.05$  was observed. This signal can be attributed to the superoxide ion formed when an oxide ion near the surface traps a hole, (see equation (2)), as reported in previous studies.<sup>27,29,31</sup> Thus, holes photogenerated by the UV light irradiation caused the signal in the range of  $g = 2.03 \sim 2.05$ .



The ESR spectrum of the Pt/YSZ powder catalyst in the  $\text{CH}_4$  atmosphere and UV light irradiation (red line) showed a decrease in the signal in the range of  $g = 2.03 \sim 2.05$  compared to the spectrum in the  $\text{N}_2$  atmosphere (blue line). The decrease in the signal in Figure 4(b) indicated that the photogenerated holes were used for the reaction with  $\text{CH}_4$ .

Figure S14 shows the transfer model of photogenerated carriers in the Pt/YSZ powder catalyst under the  $\text{CH}_4$  atmosphere and UV light irradiation, as inferred from the ESR spectra. The photogenerated electrons by the UV light irradiation were transferred to Pt and were used for the reduction reaction. On the other hand, the photogenerated holes were used for the oxidation reaction with  $\text{CH}_4$ . In addition, this transfer model of photogenerated carriers can occur in the SRM using the GPEC system with separate reaction sites.

The GPEC system used in this study, allowed analysis of the oxidation and reduction sites separately, and was useful for providing design guidelines for photocatalysts and for analyzing the reaction mechanism. For instance, hollow nanostructured photocatalysts are particularly advantageous for strategic design. Various hollow nanostructured photocatalysts have been studied so far.<sup>32,33</sup> One of the advantages of hollow nanostructured photocatalysts is that redox reactions are promoted and their reverse reactions are suppressed because the hollow nanostructures allow the separation of oxidation and reduction sites and different co-catalysts can be loaded on the inside and outside of the hollow nanostructures.<sup>32,33</sup> However, the behavior of photogenerated electrons and holes during the reaction and the reaction mechanism, which are necessary for reasonably designing hollow nanostructured photocatalysts, are less understood.<sup>32</sup> We therefore expect that the findings obtained through the GPEC system in this study will be useful in providing design guidelines for hollow nanostructured photocatalysts with ionic conductivity, where ions act as mediators of the reactions.

In this study, we separated the reaction sites for SRM to suppress the side reaction (CO<sub>2</sub> generation) using the GPEC system, allowing light irradiation of the cell fabricated by screen printing the Pt/YSZ powder catalyst on the YSZ pellet. As a result, SRM occurred stoichiometrically, and the production of CO<sub>2</sub> was successfully suppressed. In the GPEC system, oxygen ions act as mediators for SRM. The reaction had been promoted by UV light irradiation, and its effect was found to exist on both the anode and cathode sides, which is different from the trend found in a previous DRM study.<sup>18</sup> The ESR results indicated that photogenerated electrons were transferred to Pt and used for the H<sub>2</sub> evolution reaction, while photogenerated holes reacted with CH<sub>4</sub> in the SRM. The GPEC system used in this study enabled the analysis of oxidation and reduction sites separately. Therefore, we expect that the findings obtained through the GPEC system will be useful in providing design guidelines for other photocatalysts, such as hollow nanostructured catalysts with ionic conductivity, where ions act as mediators for the reactions.

This study was supported by JST-CREST (No. JPMJCR15P1). We appreciate Mr. Genseki at the Open Facility Center, Tokyo Institute of Technology, for his TEM analysis. We would like to thank Editage (www.editage.com) for English language editing.

## Conflicts of interest

There are no conflicts to declare.

## Notes and references

- 1 U.S. Energy Information Administration, U.S. Shale Production.
- 2 2015 Edo Rizky Wiyono, *J. Chem. Inf. Model.*, 2013, **53**, 1689–1699.
- 3 J. M. Lavoie, *Front. Chem.*, 2014, **2**, 1–17.
- 4 H. Arakawa, M. Aresta, J. N. Armor, M. A. Barteau, E. J. Beckman, A. T. Bell, J. E. Bercaw, C. Creutz, E. Dinjus, D. A. Dixon, K. Domen, D. L. DuBois, J. Eckert, E. Fujita, D. H. Gibson, W. A. Goddard, D. W. Goodman, J. Keller,

- G. J. Kubas, H. H. Kung, J. E. Lyons, L. E. Manzer, T. J. Marks, K. Morokuma, K. M. Nicholas, R. Periana, L. Que, J. Rostrup-Nielsen, W. M. H. Sachtler, L. D. Schmidt, A. Sen, G. A. Somorjai, P. C. Stair, B. Ray Stults and W. Tumas, *Chem. Rev.*, 2001, **101**, 953–996.
- 5 N. A. K. Aramouni, J. G. Touma, B. A. Tarboush, J. Zeaiter and M. N. Ahmad, *Renew. Sustain. Energy Rev.*, 2018, **82**, 2570–2585.
- 6 T. L. Levalley, A. R. Richard and M. Fan, *Int. J. Hydrogen Energy*, 2014, **39**, 16983–17000.
- 7 D. Mateo, J. L. Cerrillo, S. Durini and J. Gascon, *Chem. Soc. Rev.*, 2021, **50**, 2173–2210.
- 8 H. Yoshida, K. Hirao, J. I. Nishimoto, K. Shimura, S. Kato, H. Itoh and T. Hattori, *J. Phys. Chem. C*, 2008, **112**, 5542–5551.
- 9 Y. Cho, A. Yamaguchi and M. Miyauchi, *Catalysts*, 2021, **11**, 1–41.
- 10 B. Han, W. Wei, L. Chang, P. Cheng and Y. H. Hu, *ACS Catal.*, 2016, **6**, 494–497.
- 11 H. Song, X. Meng, Z. J. Wang, Z. Wang, H. Chen, Y. Weng, F. Ichihara, M. Oshikiri, T. Kako and J. Ye, *ACS Catal.*, 2018, **8**, 7556–7565.
- 12 B. V. Ayodele, A. A. Ghazali, M. Y. Mohd Yassin and S. Abdullah, *Int. J. Hydrogen Energy*, 2019, **44**, 20700–20710.
- 13 L. Yuliaty, H. Itoh and H. Yoshida, *Chem. Phys. Lett.*, 2008, **452**, 178–182.
- 14 H. Song, X. Meng, T. D. Dao, W. Zhou, H. Liu, L. Shi, H. Zhang, T. Nagao, T. Kako and J. Ye, *ACS Appl. Mater. Interfaces*, 2018, **10**, 408–416.
- 15 Y. Cho, S. Shoji, A. Yamaguchi, T. Hoshina, T. Fujita, H. Abe and M. Miyauchi, *Chem. Commun.*, 2020, **56**, 4611–4614.
- 16 S. Shoji, X. Peng, A. Yamaguchi, R. Watanabe, C. Fukuhara, Y. Cho, T. Yamamoto, S. Matsumura, M. W. Yu, S. Ishii, T. Fujita, H. Abe and M. Miyauchi, *Nat. Catal.*, 2020, **3**, 148–153.
- 17 Miyauchi et al. Japan patent application, JP2018–156558.
- 18 M. Kushida, A. Yamaguchi, Y. Cho, T. Fujita, H. Abe and M. Miyauchi, *ChemPhotoChem*, 2020, 1–8.
- 19 C. J. Liu, J. Ye, J. Jiang and Y. Pan, *ChemCatChem*, 2011, **3**, 529–541.
- 20 S. B. Tang, F. L. Qiu and S. J. Lu, *Catal. Today*, 1995, **24**, 253–255.
- 21 P. Sun, B. Young, A. Elgowainy, Z. Lu, M. Wang, B. Morelli and T. Hawkins, *Environ. Sci. Technol.*, 2019, **53**, 7103–7113.
- 22 V. R. Paiverneker, A. N. Petelin, F. J. Crowne and D. C. Nagle, *Phys. Rev. B*, 1989, **40**, 8555–8557.
- 23 U. Vohrer, H. D. Wiemhöfer, W. Göpel, F. Schilling and J. Arndt, *Sensors Actuators B. Chem.*, 1991, **4**, 411–416.
- 24 S. Gordon and B. J. McBride, 1994, 58.
- 25 M. Maczka, E. T. G. Lutz, H. J. Verbeek, K. Oskam, A. Meijerink, J. Hanuza and M. Stuiyinga, *J. Phys. Chem. Solids*, 1999, **60**, 1909–1914.
- 26 Q. Zhao, X. Wang and T. Cai, *Appl. Surf. Sci.*, 2004, **225**, 7–13.
- 27 J. Zhang, Y. Gao, X. Jia, J. Wang, Z. Chen and Y. Xu, *Sol. Energy Mater. Sol. Cells*, 2018, **182**, 113–120.
- 28 J. M. Costantini, F. Beuneu and W. J. Weber, *Philos. Mag.*, 2014, **94**, 2281–2296.
- 29 C. Gionco, M. C. Paganini, E. Giamello, R. Burgess, C. Di Valentin and G. Pacchioni, *Chem. Mater.*, 2013, **25**, 2243–2253.
- 30 H. Liu, L. Feng, X. Zhang and Q. Xue, *J. Phys. Chem.*, 1995, **99**, 332–334.
- 31 A. Martínez-Arias, M. Fernández-García, C. Belver, J. C. Conesa and J. Soria, *Catal. Letters*, 2000, **65**, 197–204.
- 32 M. Xiao, Z. Wang, M. Lyu, B. Luo, S. Wang, G. Liu, H. M. Cheng and L. Wang, *Adv. Mater.*, 2019, **31**, 1–23.
- 33 D. Zheng, X. N. Cao and X. Wang, *Angew. Chemie - Int. Ed.*, 2016, **55**, 11512–11516.